The Role of Chelating Phosphine Rhodium Complexes in Dehydrocoupling Reactions of Amine-Boranes: A Theoretical Investigation Attempting To Rationalize the Observed Behaviors

Valeria Butera, Nino Russo, and Emilia Sicilia*

Dipartimento di Chimica e Tecnologie Chimiche, Università della Calabria, 87036 Arcavacata di Rende (CS), Italy

Ⓢ *Supporting Information*

ABSTRACT: A quantum-chemical investigation of the dehydrocoupling reaction of the secondary amine-borane Me_2HNBH_3 assisted by phosphine chelating $[Rh(Ph_2P(CH_2)_n\text{-}PPh_2)(C_6H_5F)]^+$ (n = 3−5) complexes to ultimately afford the cyclic dimer $[Me_2NBH_2]_2$ is reported. The hypothesis, proposed on the basis of experimental evidence, that the catalytic efficiency of such systems is due to formation of Rh(III) dihydride complexes, which rapidly lose H_2 and reform Rh(I) species, has been explored, together with the influence that the structure of the ligand (namely, the chelating phosphine P−Rh−P bite angle) has on the rate of the reaction. Along the pathway that our computational analysis has indicated as the most likely, the first step of the dehydrogenation reaction is the concerted B−H hydride and N−H proton transfer from an additional amine-borane molecule to the rhodium center of the formed $[Rh(Ph_2P(CH_2)_n\text{-}PPh_2)(\eta_2\text{-}Me_2HNBH_3)]^+$ complexes. The reaction proceeds by formation of dihydrogen complexes, which eliminate molecular hydrogen and restore the σ-amine-borane complexes. The impact of the bite angle on the kinetics has been rationalized in terms of both the distortions to the geometry of stationary points around the metal center and the strength of the Rh−B interaction with the amine-borane ligand. The final cyclic dimer is formed by off-metal coupling of the released aminoboranes. A plausible explanation of the observed induction period is also given.

KEYWORDS: amine-boranes dehydrogenation, chelating phosphine, rhodium complex, DFT, homogeneous catalysis
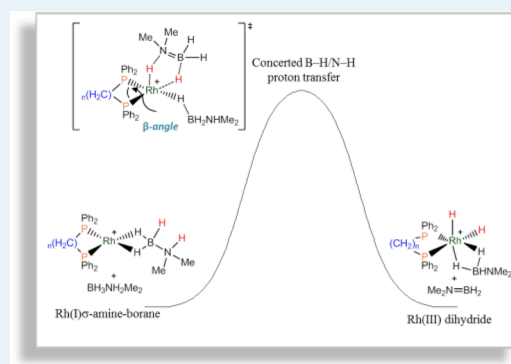
1. INTRODUCTION

The potential use of hydrogen as a clean and abundant fuel source for energy generation has driven a recent intense research effort toward the use of ammonia-borane (AB), H_3NBH_3, and related amine-boranes (R_2HNBH_3) as safe and easily manipulated compounds for chemical storage of H_2.[1−4] Although the combination of hydridic B−H and protic N−H bonds within the AB and amine-borane molecules mean that they are susceptible to thermally induced hydrogen release, the temperatures at which this occurs are impractically high (110−200 ∘C). This factor has, in turn, resulted in a focus upon the use of catalytic methods to cause hydrogen evolution and concomitant B−N bond formation for the AB molecule itself, and for a wide variety of di- and monoalkylamine borane molecules. Experimental and theoretical investigations carried out so far have shown that metal-mediated dehydrocoupling reactions of amine-boranes are very complex processes and both the mechanism and the final outcome depend on the nature of the catalyst in terms of identity of the metal center, ligands and bonding modes. The nature of the amine-borane alkyl groups also influences the course of the process. In this respect, mechanistic investigations are more undemanding when secondary amine-boranes are used because of the limited number of possible products that can be formed on dehydrogenation. This is the reason why there is today a great

number of catalytic systems of elements from different zones of the periodic table, which have been proved to be able to assist the dehydrocoupling of the secondary amine-borane Me_2HNBH_3 (**A**) to give the cyclic dimer $[Me_2NBH2]_2$ (**C**).[5−25] According to the schematic representation given in Scheme 1, a number of

Scheme 1. Hypothesized Intermediates and Products of the Dehydrocoupling Reaction of Amine-Boranes Assisted by Metal Catalysts
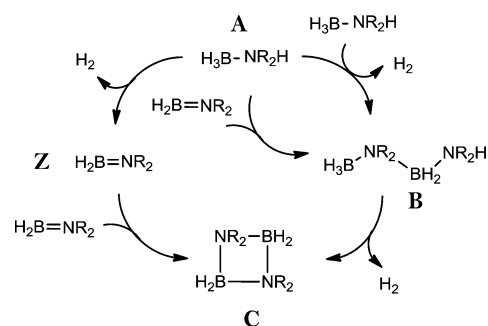
mechanistic regimes have been suggested by the detection of several boron−nitrogen intermediates: formation of the aminoborane $H_2B=NMe_2$ (**Z**) by dehydrogenation of **A**; coupling of **A** and **Z**, or of two **A** to form, by elimination of H_2, the intermediate linear diborazane **B**; and formation of the dimeric final product **C** by both dimerization of **Z** and dehydrocyclization of **B**. Diborazane **B** can be consumed also by B−N bond cleavage.

Neither is the explicit role played by the metal in each step given in such scheme nor are all the sketched pathways operative for each catalytic system. Concerning the role of the metal complex in such transformations, there are two viable general pathways: The so-called on-metal, in which the amine-borane coordinates to the metal center and undergoes H transfers with or without the direct involvement of the metal by a variety of mechanistic steps. BH and NH hydrogen atoms can be eliminated from the same molecule when the mechanism is intramolecular, whereas the process is intermolecular when the two hydrogen atoms belong to different molecules. The mechanistic steps are defined off-metal if the metal complex does not participate in the reaction.

It should be desirable to combine all such mechanistic possibilities, together with the role played by the metal in each of the involved steps, in a unified model broadly applicable to many of the used catalysts. Very recently, Weller and co-workers, on the basis of the outcomes of a detailed study of isolated intermediates, catalysis, stoichiometric reactivity, and kinetic simulation using a rhodium catalyst system, have postulated a simplified and largely applicable mechanistic scheme that should be helpful in rationalizing the behavior of many transition-metal and main-group systems that catalyze the dehydrocoupling of **A** to afford the cyclic amino-borane dimer **C**.[26] A key aspect of such a multifaceted and complex mechanistic scheme is the possibility for the involved cationic rhodium catalyst to shuttle between a fast Rh(I)/Rh(III) regime and a slower constant oxidation state rhodium(III) dihydride regime. Indeed, by dehydrogenation of bound **A**, a dihydride intermediate $M(H)_2$ can be formed to give **Z**. If H_2 loss from the dihydride complex is slow, this species becomes the resting state of the process. In this mechanistic scenario, **C** is invoked as a modifier, which acts in an autocatalytic way, moving the system between the slow rhodium(III) dihydride regime and the fast Rh(I) regime by promoting reductive elimination of H_2.

[Rh(chelating bis-phosphine)] systems have been proved[27] to be extremely efficient catalysts for the dehydrogenation of **A** to ultimately form **C**. When systems such as [Rh-$(Ph_2PCH_2CH_2CH_2PPh_2)$]$^+$ are used to assist the dehydrocoupling process, turnover rates are 2 orders of magnitude faster than reported for monodentate phosphine catalysts. To explain such behavior, the authors have postulated that the Rh(III) dihydride complex formed by dehydrogenation of bound **A**, with the concomitant change in the oxidation state, rapidly loses H_2 and reforms a Rh(I) species. The combined effects of relative instability of Rh(III) dihydride intermediates, lack of ligand flexibility and P−Rh−P bite angle, defined as the preferred chelation angle determined by the ligand backbone only,[28] have been considered to be responsible of the observed efficiency. In particular, the influence of the chelate ligand backbone on reactivity has been investigated by considering the relative rates of dehydrocoupling of **A** assisted by the bisphosphine chelating complexes $[Rh(Ph_2P(CH_2)_n\text{-}PPh_2)(C_6H_5F)][BAr^F_4]$ with $n = 3-5$. A structural analysis carried out on a great number of bidentate ligands to parametrize their coordinating properties[29] has allowed the estimation of the bisphosphine ligand bite angle

and bite, given as the distance between the two donor atoms when coordinated, for the involved complexes. The catalyst with $n = 3$, corresponding to the estimated smallest chelate bite-angle, is found to be the fastest, and the catalyst with $n = 5$ is the slowest. Moreover, there is an induction period associated with this catalysis that the authors suggest can be due to the formation of an inactive dimeric species (Scheme 2) possibly in equilibrium with monometallic active species.

Scheme 2. Proposed Mechanism for the Dehydrogenation of A Assisted by Bidentate Phosphine Complexes $[Rh(Ph_2P(CH_2)_n\text{-}PPh_2)(C_6H_5F)][BAr^F_4]$ $(n = 3-5)^a$
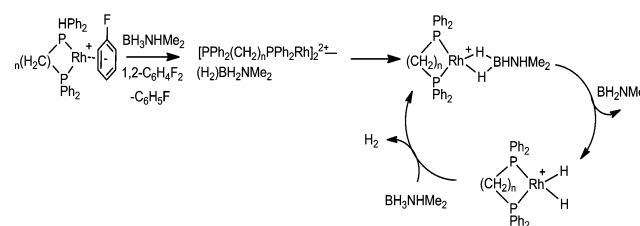
$^a[BArF_4]^-$ anions are not shown.

In this paper, the outcomes of a systematic density functional theory (DFT) investigation of the possible mechanistic routes of dehydrocoupling of the prototypical secondary dimethylamine-borane **A** assisted by Rh-chelating bisphosphine complexes $[Rh(Ph_2P(CH_2)_n\text{-}PPh_2)(C_6H_5F)]^+$ $(n = 3-5)$ are reported. Even though such complexes are the organometallic precatalysts in $1,2\text{-}C_6H_4F_2$ solvent, the mechanistic investigation really starts from the corresponding $[Rh(Ph_2P(CH_2)_n\text{-}PPh_2)(\eta_2\text{-}Me_2HNBH_3)]^+$ complexes that are formed by displacement of the labile fluoroarene ligand and η_2 coordination of Me_2HNBH_3.

Calculations have been carried out with the support of the experimental observations and hypotheses concerning the reaction mechanism. The assumption that in going from $n = 3$ to $n = 5$, the enlargement of the P−Rh−P bite angle corresponds to tighter Rh−B interactions and, as a consequence, to slower catalysis, has been tested with the aim to confirm the supposed relationship between structure and reactivity, very helpful for the development of tailored catalysts. Such a correlation between the bite angle of bidentate ligands, specifically bidentate phosphines, and the catalytic activity of their complexes has been previously explored both theoretically and experimentally, and the advantages deriving from the use of diphosphine chelating ligands in homogeneous catalysis is still a matter of debate.[30−36] The results of the rigorous computational analysis reported here of the mechanistic scheme suggested on the basis of experimental evidence aims to establish how bidentate phosphine ligand bite angles affect the performance in catalysis of their complexes. Moreover, the present computational exploration of the mechanistic aspects of the amine-boranes dehydrocoupling process catalyzed by Rh(chelating bisphosphine) complexes furnishes additional details to the more general context of metal-assisted amine-borane dehydrogenation processes.

2. COMPUTATIONAL DETAILS

All DFT calculations in this study have been performed using the Gaussian 03 suite of ab initio programs[37] employing the hybrid XC functional B3PW91.[38] For Rh, the relativistic compact Stuttgart/Dresden effective core potential[39] has been used in conjunction with its split valence basis set. The standard 6-311G* basis sets of Pople and co-workers have been employed

for the rest of the atoms, except C and H atoms of phenyl rings, for which the smaller 6-31G basis sets have been used. A series of preliminary calculations has been carried out to ascertain whether weak dispersion interactions can have an influence on the shape of the calculated energy profiles. The energetics of critical regions of potential energy surfaces (PESs) recalculated by using the ωB97XD functional,[40] a range-separated version of Becke's 97 functional,[41] do not show any significant change when dispersion corrections are accounted for. The geometric structures of all complexes studied in this paper have been optimized as gas-phase as the cation only. Calculating the harmonic vibrational frequencies at the optimized structures and noting the number of imaginary frequencies have confirmed the nature of all intermediates (no imaginary frequency) and transition states (only one imaginary frequency), which also have been confirmed to connect reactants and products by the intrinsic reaction coordinate (IRC)[42] calculations. The zero-point energy (ZPE) and entropic contribution have been estimated within the harmonic potential approximation. The enthalpies, H, and free energies, G, have been calculated for $T = 298.15$ K.

Because the real entropic cost under catalytic conditions is not properly reproduced by using this method and the effects are particularly relevant for the substrate association and dissociation,[43] following a common approach in theoretical catalysis, the solvation entropy has been estimated as two/thirds of its gas-phase value.[43,44] All relative energies are reported in kilocalories per mole. Because preliminary calculations have clearly shown that geometry relaxation effects are not significant, the solvation Gibbs free energies have been calculated in implicit isoquiniline ($\varepsilon = 11.0$), as a mimic of the 1,2-$F_2C_6H_4$ solvent, using the integral equation formalism polarizable continuum model (IEFPCM),[45] performing single point calculations on gas-phase optimized structures. Reaction Gibbs free energies in solution, ΔG_{sol}, have been calculated for each process, using the well-known thermodynamic cycle,[46] as the sum of two contributions: a gas-phase reaction free energy, ΔG_{gas}, and a solvation reaction free energy term calculated with the continuum approach, ΔG_{solv}. The gas-phase reaction free energy was calculated as illustrated above. In the beginning, an exploration of all the plausible reaction pathways, with the purpose to identify the most favorable one, was carried out by using a simplified model of the $[Rh(Ph_2P(CH_2)_2\text{-}PPh_2)(C_6H_5F)]^+$ complex. Indeed, to reduce the required computational effort, at this stage of the computational analysis, the phenyl rings of phosphine ligands have been replaced with less demanding methyl groups. For the studied complexes, from now on, we will adopt the same nomenclature used originally by the authors.[27] In particular, $[Rh(Ph_2P(CH_2)_n\text{-}PPh_2)(C_6H_5F)]^+$ complexes will be labeled **1b**, **1c**, and **1d** for $n = 3$, $n = 4$ and $n = 3$, respectively. The corresponding $[Rh(Ph_2P(CH_2)_n\text{-}PPh_2)(\eta_2\text{-}Me_2HNBH_3)]^+$ complexes formed by addition of Me_2HNBH_3, and displacement of the labile fluoroarene ligand, will be labeled **2b**, **2c** and **2d**. The simplified model of **2b**, used to predict the lowest energy pathway, will be indicated as **2b(Me)**.

3. RESULTS

All the energy profiles describing the results of our computational analysis carried out by focusing on the simplified catalyst model **2b(Me)** are reported in terms of relative gas-phase zero-point corrected energies. Free energy profiles in solution, instead, are reported to illustrate the outcomes of the investigation of the dehydrogenation reaction for **2b**, **2c**, and **2d** complexes. Along

the reaction pathways, the optimized structures of intercepted intermediates and transition states are shown, whereas complete geometric information is reported in the Supporting Information (SI). Scheme 3 provides an overview of all the possible reaction

Scheme 3. Overview of All Selected Viable Dehydrocoupling Pathways
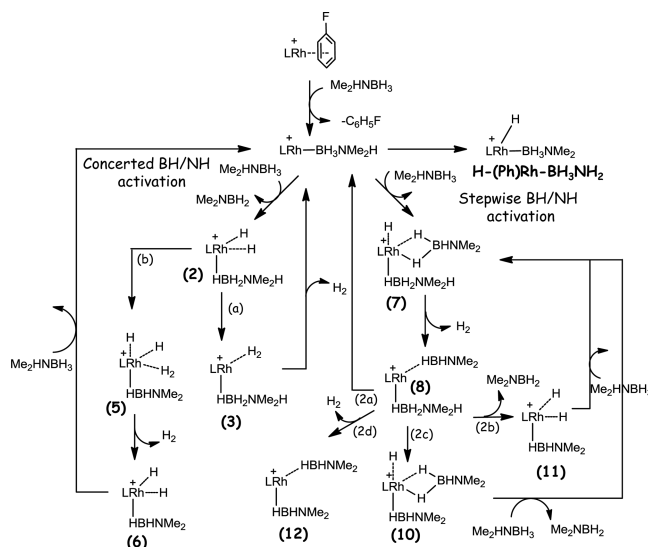
routes that appear to be viable on the basis of both experimental findings and computational results and have been selected as a function of the energetics of the intercepted minima and transition states. Even though complex **1** is the organometallic precatalyst in fluorobenzene solvent, the mechanistic investigation really starts from the complex formed by addition and coordination of the Me_2HNBH_3 substrate, which causes the displacement of the bound arene solvent in **1**.

3.1. Formation of Dimeric Species. At the very beginning of our investigation the attention was focused on the hypothesis that the formation of a dinuclear metal−metal bonded complex in equilibrium with the mononuclear active species (see Scheme 2) could be responsible for the observed induction period. Experimental findings confirm an inverse relationship between the induction period and the catalyst loading, at constant substrate concentration. Such a hypothesis is supported by the isolation of a dicationic dimer formed from two monodentate phosphine fragments bridged by three H_3BNMe_3 ligands,[47] as well as by the observation of induction periods in homogeneous systems that invoke equilibria between active monomeric species and inactive polymetallic species.[48] The authors also suggest that formation of a dicationic dimer requires prior substrate activation, and anyhow, experiments do not allow drawing of firm conclusions.

All the suitable computational strategies and all the possible starting assemblies of monomers (e.g., with and without fluoroarene units) have been employed to examine this hypothesis. All the attempts to model a pathway that from the initially reacting monomeric species leads to the formation of the dimer have been unsuccessful. The monomers unavoidably tend to stay apart and, plausibly, either particular experimental conditions or reacting species different with respect to the complexes examined here are required to form a dinuclear complex. Nevertheless, in consideration of the role that such a complex should play in transition-metal catalyzed amine-boranes dehydrocoupling,[47] we have investigated what might happen

once the dimeric complex is formed, whatever the mechanism and appropriate operative conditions.

The energy profile reported in Figure 1 shows minima and connecting transition states intercepted along a viable dehydro-
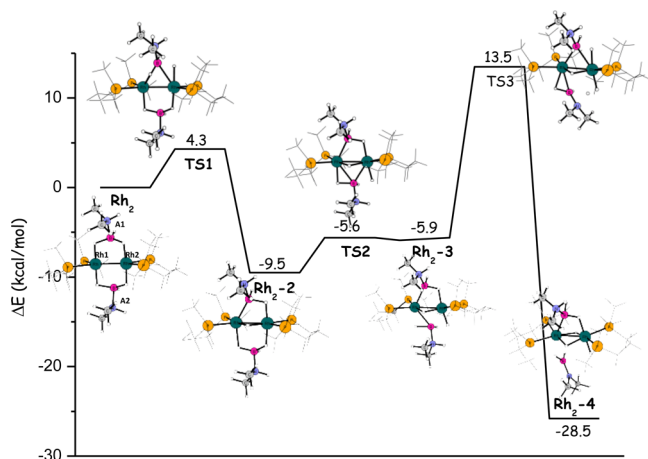

Figure 1. Calculated B3PW91 gas-phase zero-point-corrected energy profile for the dehydrogenation reaction of amine-borane ligands in the dicationic dimeric complex labeled Rh$_2$. Energies are in kilocalories per mole and relative to the reactants' asymptote.

genation pathway. The optimized structure of the dicationic dimeric species, Rh$_2$, formed from two $[Rh(Me_2P(CH_2)_3$-$PMe_2)]^+$ fragments bridged by two **A** ligands, is reported in Figure 1. Such a structure is consistent with that reported for a dirhodium silyl complex.[46] Full details of the optimized structures are reported in the Supporting Information (S1). The two rhodium atoms are bridged by two activated B−H hydrogen atoms for each **A** ligand. The Rh−Rh bond length is 2.515 Å consistent, even if shorter, with that for a single bond distance. Both rhodium centers adopt a distorted bipyramidal trigonal geometry. With respect to the monomeric rhodium sigma complex of $H_3B \cdot NMe_3$ **2b(Me)**, the Rh$_2$ complex is calculated to be less stable by 29.8 kcal/mol. Very similar values of the endothermicity of the formation reaction of the dimeric species by two $[Rh(Ph_2P(CH_2)_n-PPh_2)]^+$ fragments bridged by two **A** ligands have been calculated for $n = 1-3$. Computed values are 31.3, 30.9, and 28.6 kcal/mol for $n = 1$, $n = 2$, and $n = 3$, respectively. Moreover, all the attempts to locate a low-energy practicable route leading from the intercepted dimeric species to the formation of separate **2b(Me)** fragments have failed.

Along the pathway sketched in Figure 1 the first step, which occurs by surmounting an energy barrier of about 4 kcal/mol, is the shift of a hydrogen from the dimethylamine-borane ligand, labeled **A1**, to rhodium. In the formed intermediate, the hydrogen atom occupies a bridged position between the two rhodium atoms.

The next step consists of another hydrogen atom shift from the **A** molecule, labeled **A2**, to Rh$_2$ with concomitant detachment of the ligand **A1** from Rh$_2$. The barrier height is 3.9 kcal/mol. and the formed intermediate is only slightly more stable. The height of the barrier for the last step of the process, which leads to the elimination of an amino-borane molecule. is 19.4 kcal/mol. As a result of the interaction of the hydride on Rh$_2$ and a NH proton of ligand **A2**, which seems to lead to the formation of a H$_2$ molecule, a very stable dimer is formed. The molecular structure of such a complex, which lies ~28 kcal/mol below the entrance channel of the reaction, consists of one distorted octahedral

rhodium center linked to a pseudosquare pyramidal rhodium center. The two Rh atoms lie at a distance of 2.621 Å and are bridged by two hydride ligands in equatorial positions. Finally, an aminoborane molecule is eliminated, but neither molecular hydrogen nor separate **2b(Me)** fragments are formed. Thus, the potential formation of the dimeric species inhibits the dehydrogenation reaction. It is worth underscoring that all the indications coming from our computational analysis exclude that dimeric species are involved in the process. In the next sections, the most plausible reaction mechanism will be illustrated, and a tentative explanation will be given of the observation of an induction period.

3.2. Selection of the Me$_2$HNBH$_3$ Dehydrogenation Reaction Pathway.

Experimental findings suggest that when [Rh(chelating bisphosphine)] catalysts assist the dehydrocoupling process, the formation of **Z** occurs by dehydrogenation of **A** with formation of a Rh(III) dihydride intermediate and change in oxidation state at Rh, followed by rapid loss of H$_2$ to reform a Rh(I) species. Experiments have also shown that linear dimer Me$_2$HNBH$_2$NMe$_2$BH$_3$ is not an intermediate. Given the potential complexity of the reaction steps required to afford the final product **C**, an initial exploration of all the plausible reaction pathways has been carried out by using the catalyst model **2b(Me)**. All the Cartesian coordinates of stationary points along the examined reaction pathways illustrated in Figures 2−4 are given in Figure S2 of SI.
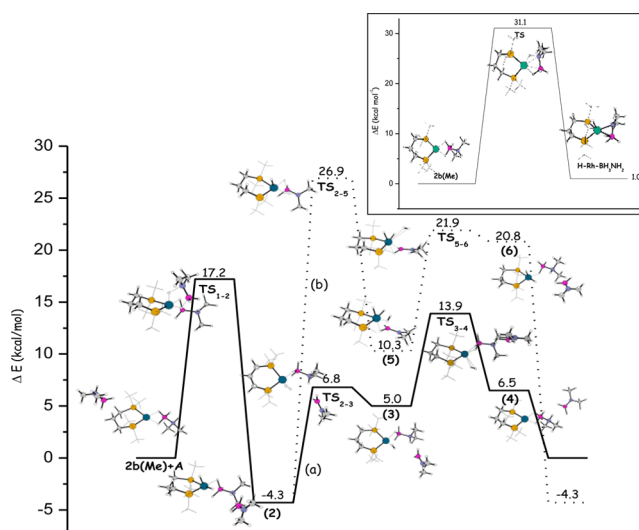

Figure 2. Calculated B3PW91 zero-point corrected energy profiles for the dehydrogenation reaction, which involves concerted NH/BH activation as the first step, of a dimethylamine-borane molecule A assisted by the model catalyst **2b(Me)**. Along the path labeled a, a dihydrogen ligand in equatorial position coordinated with the Rh center is formed, whereas hydrogen transfer from the bound **A** molecule occurs along path b. In the right upper side is reported the pathway for the hydrogen transfer occurring after coordination of one molecule of the DMAB substrate. Energies are in kilocalories per mole and relative to the reactants' asymptote.

According to clues coming from experiments, at first, all the efforts were devoted to computing a path leading to the formation of a Rh dihydride complex. Direct transfer of hydrogen atoms from the coordinated **A** molecule to the rhodium center in complex **2b(Me)** does not occur. Indeed, as shown in the framework on the right-upper side in Figure 2, once a substrate DMAB molecule displaces the fluoroarene ligand coordinating to
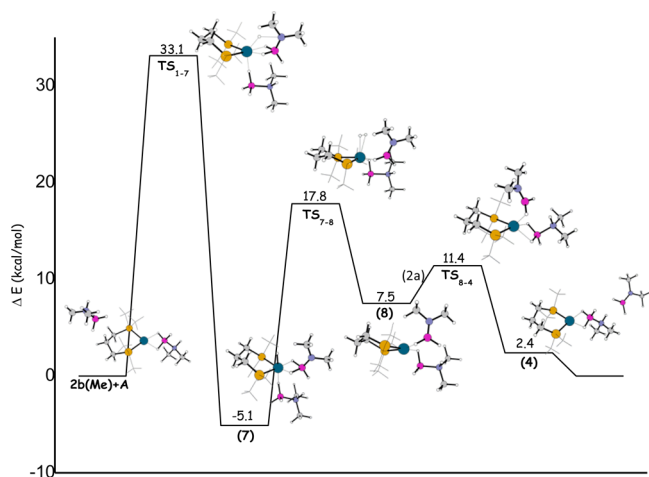
Figure 3. Calculated B3PW91 zero-point-corrected energy profiles for the dehydrogenation reaction, which involves stepwise NH/BH activation as the first step, of the bound dimethylamine-borane molecule **A** in model complex **2b(Me)** assisted by a second **A** molecule. Energies are in kilocalories per mole and relative to the reactants' asymptote.
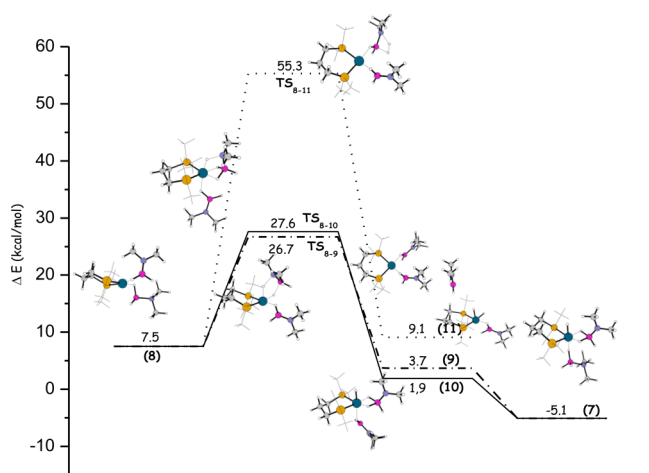

Figure 4. Calculated B3PW91 zero-point energy profiles for the different dehydrogenation pathways that from intermediate 8 lead to the regeneration of intermediate 7 along **2b** and **2c** and formation of the diaminoborane intermediate 11 along **2d**. Energies are in kilocalories per mole and relative to the reactants' asymptote.

the metal center in an η^2 fashion, a NH proton can be transferred to the metal. The height of the barrier for this NH proton shift is 31.1 kcal/mol, and the minimum that is formed is ~1 kcal/mol less stable than the reference **2b(Me)** complex. Despite the favorable geometrical assembly of the intermediate H-(Me)Rh-NH$_2$BH$_3$, which seems to lead up to the transfer of the BH hydride to the Rh center, dehydrogenation and formation of a dihydride intermediate does not occur.

All the attempts carried out with the purpose of intercepting a transition state for a BH hydride shift have been unsuccessful. Geometric constraints imposed by the presence of the chelating diphosphine ligand hamper the second hydrogen atom transfer. Therefore, once intermediate H-(Me)Rh-NH$_2$BH$_3$ is formed, the reaction is blocked, and the process cannot proceed. Only when a second amine-borane molecule interacts with the **2b(Me)** complex does the dehydrogenation process start. The pathway for the formation of the monohydride intermediate H-(Me)Rh-BH$_3$NH$_2$ leads nowhere and can be assumed to be

responsible for the observation of an induction period. On the contrary, following the reaction of the **2b(Me)** complex with an additional DMAB molecule, the reaction pathway bifurcates, as we are going to illustrate.

The first step of the pathways shown in Figure 2 is the concerted BH/NH activation of the second amine-borane molecule approaching the complex. The dehydrogenation proceeds by hydrogen transfer to the metal center through the transition state **TS$_{1-2}$**, with an energy barrier of 17.2 kcal/mol, to afford the Rh dihydride intermediate (**2**) that is more stable by 4.3 kcal/mol than **2b(Me)+A**. A H$_2$B=NMe$_2$ molecule is eliminated, and the Rh center assumes a pseudo-octahedral geometry, thanks to the η^2-coordinatation of the remaining amine-borane ligand. Along an alternative and less productive dehydrogenation pathway, which is shown in Figure 3, the second amine-borane molecule can assist the stepwise NH and BH bonds' activation of the bound **A** molecule.

The first H transfer from the N atom to the Rh center occurs through the transition state **TS$_{1-7}$** by overcoming a high energy barrier of 33.1 kcal/mol. In the formed intermediate 7, which lies 5.1 kcal/mol below the reactants' asymptote, the second **A** molecule is η^1-coordinated to the metal center in an axial position. The subsequent BH hydride shift does not lead to the formation of a dihydride complex. Indeed, the two H atoms interact to directly produce and release molecular hydrogen. The intermediate (**8**) that is formed is less stable by 12.6 kcal/mol than the previous intermediate. The geometry at the Rh center in intermediate 8 is pseudo-square-planar, with ligands **A** and the formed **Z** coordinated in η^1 fashion. Such an intermediate is afforded through the transition state **TS$_{7-8}$** by surmounting an energy barrier of 22.9 kcal/mol.

The outcomes of the computational analysis carried out so far clearly show that the pathway for the concerted dehydrogenation leading to the formation of intermediate **2** is more favorable and accessible in practice than the stepwise dehydrogenation affording intermediate **8**. Nevertheless, all the accessible routes from both intermediate **2** and **8** have been examined. The two noncompetitive pathways that begin with the formation of **2** are described in Scheme 4, and the corresponding calculated energy profiles are shown in Figure 2. After formation of the dihydride complex, the reaction proceeds along the low-energy path, labeled a, by formation of a dihydrogen ligand in equatorial position coordinated with the Rh center that has a pseudo-square-planar geometry. The minimum (**3**) lies 5.0 kcal/mol

Scheme 4. Overview of All the Selected Viable Dehydrogenation Pathways Originating from Intermediate 2
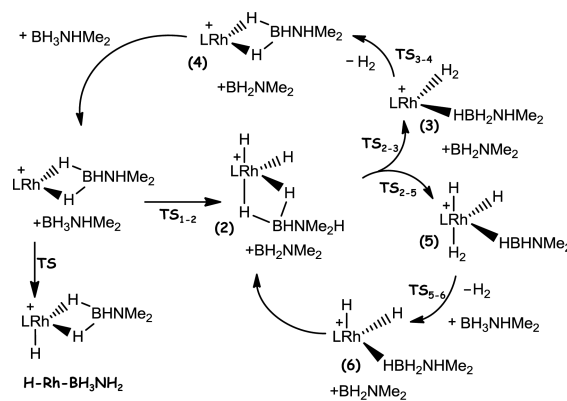
above the reactants' dissociation limit, and the height of the barrier leading to it is 11.1 kcal/mol.

The next step, that is, loss of molecular hydrogen, regenerates the **2b(Me)** complex, and the addition of a new **A** molecule restarts the catalytic cycle. Alternatively, along the second pathway, labeled b, the reaction mechanism involves the concerted NH proton and BH hydride shifts from the bound amino-borane to the metal center in axial and equatorial positions, respectively. As a consequence, the geometry at the Rh center of the formed (**5**) intermediate becomes pseudo-octahedral, with the formed hydrogen molecule as the sixth ligand in the equatorial position and the dehydrogenated amino-borane molecule adopting an η^1 coordination. Intermediate **5**, which is less stable by 14.6 kcal/mol than the preceding intermediate, can be accessed through **TS$_{2-5}$**, by overcoming an energy barrier of 31.2 kcal/mol. The loss of the H$_2$ molecule from intermediate **5** occurs with a barrier of 11.6 kcal/mol and leads to the formation of an intermediate, **6**, which is more stable than **TS$_{5-6}$** by only 1.1 kcal/mol. Release of the formed amino-borane molecule and simultaneous coordination of a new **A** molecule restore intermediate **2**. Along the b pathway, therefore, the **2b(Me)** complex plays the role of precatalyst, and the catalytic cycle starts from the dihydride intermediate **2**.

All the viable alternative pathways originating from intermediate **8** have been explored. One such alternative is illustrated in Figure 3. Scheme 5 summarizes all the remaining alternatives, and Figure 4 shows the corresponding calculated free energy profiles.

Scheme 5. Overview of All the Remaining Alternative Dehydrocoupling Pathways Originating from Intermediate 8
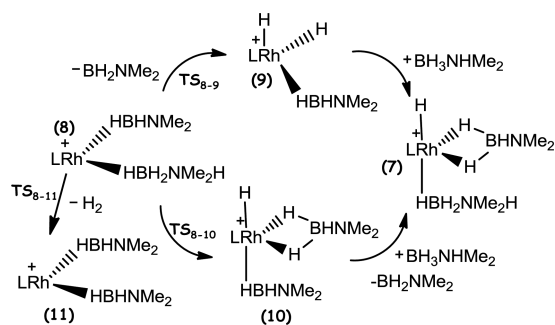
The pathway, labeled 2a, that involves the lowest energy barrier is reported in Figure 3, whereas two alternative noncompetitive pathways (2b–2c) are shown in Figure 4. Along the 2a reaction path, the **2b(Me)** complex is restored by the loss of the aminoborane molecule induced by the coordination of a new **A** ligand. The height of the calculated barrier for the corresponding transition state, **TS$_{8-4}$**, is 3.9 kcal/mol. Alternatively, along the 2b pathway, two hydrogen atoms from the ligated amine-borane molecule are transferred to the metal center by overcoming an energy barrier of 19.2 kcal/mol for the **TS$_{8-9}$** transition state. The dihydride intermediate **9** is formed, stabilized by 3.8 kcal/mol with respect the previous minimum, from which the intermediate labeled **7** in Figure 3 should be formed by coordination of a new **A** molecule and a hydride transfer from the Rh center to the dehydrogenated dimethylamine-borane ligand.

A very similar value of the energy barrier, 20.1 kcal/mol, has been calculated along the 2c path for the **TS$_{8-10}$** transition state

that corresponds to the shift of a NH proton from the amine-borane to the metal center.

The esa-coordinated minimum **10** is formed and is calculated to be more stable by 5.6 kcal/mol than intermediate **8**. Displacement of the **Z** molecule in te axial position and coordination of an additional amine-borane molecule regenerates the same **7** complex. Finally, through the very high **TS$_{8-11}$** transition state (47.8 kcal/mol) associated with the intra-molecular elimination of a H$_2$ molecule from the dimethyl-amine-borane molecule, the complex labeled **11** is formed, less stable by 1.6 kcal/mol than **8**. Although the complex **11**, which has two aminoborane molecules coordinated to the Rh atom, does not lie on a competitive pathway, its formation is noteworthy for reasons that will be illustrated below.

As a general rule, if the possibility of the formation of borazane **B** can be excluded, such as in the present case, subsequent oligomerization, polymerization or dimerization of R$_2$N=BH$_2$ can occur either on or off the metal with or without the further involvement of R$_2$HNBH$_3$. Because the observed final product of the process under investigation is the cyclic dimer **C**, the possibility that formed Me$_2$N=BH$_2$ monomers undergo further reactivity on the metal to afford **C** has been explored. Calculations carried out to model both a concerted and stepwise rearrangement mechanism leading to the formation of the **C** dimer have been unsuccessful. Although intermediate **11** should be a promising starting point for the formation of the cyclic dimer directly on the metal center, no pathway leading to such product has been calculated. According to our previous conclusions,[19] uncatalyzed dimerization in solution of the free **Z** monomers is the only way to form the dehydrocyclization product **C**.

Overall, these preliminary calculations suggest the most favorable reaction path to be that shown in Figure 2, which starts with the concerted dehydrogenation of the second noncoordinated amine-borane to yield the dihydride complex **2** and proceeds, along the pathway labeled "a", with the elimination of a H$_2$ molecule and regeneration of the initial complex **2b(Me)**. The consequence of such a result will be discussed in the next sections.

Minima and transition states along analogous pathways have been intercepted by considering the real catalytic systems **2a**, **2b**, and **2c**, with the aim of proving the suggested relationship between the amplitude of the P−Rh−P bite angle and the rate of the reaction.

3.3. Mechanistic Aspects of the Me$_2$HNBH$_3$ Dehydrogenation Assisted by 1b, 1c and 1d and Bite Angle Effect. The DFT-optimized structure of the cationic portion of the reference complex **2b** formed by addition of Me$_2$HNBH$_3$ to the [Rh(Ph$_2$P(CH$_2$)$_n$-PPh$_2$)(C$_6$H$_5$F)]$^+$ complex **1b** and displacement of the fluoroarene ligand is shown in Figure 5. Calculations confirm the square-planar geometry at the Rh(I) center and the η^2 coordination of the **A** ligand. Comparison with relevant available structural features extracted from crystallographic characterization of the complex[27] as well as with the estimated values of the bisphosphine ligand bite angle and bite[29] shows good agreement, indicating a good modeling of the catalyst.

The outcomes of the calculations for the dehydrogenation reaction are summarized in Figure 6, where the free energy profile is shown together with the fully optimized structures of stationary points. More detailed geometrical information on intercepted stationary points can be found in S3 of the SI. Gas-phase zero-point-corrected relative energies are also reported in parentheses to highlight the effects on the energetics of the replacement on the diphosphine ligand of the methyl groups,
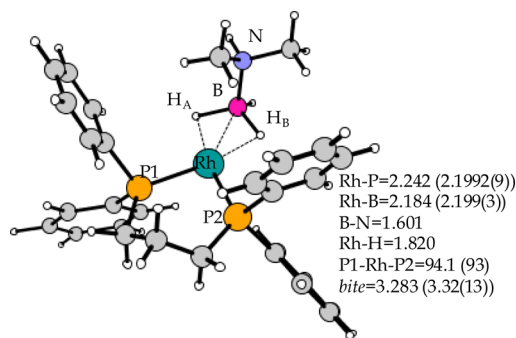
Figure 5. DFT-optimized geometrical structure of cationic portion of **2b**. Selected structural parameters (bonds in angstroms and angles in degrees) are compared with available experimental values (in parentheses).
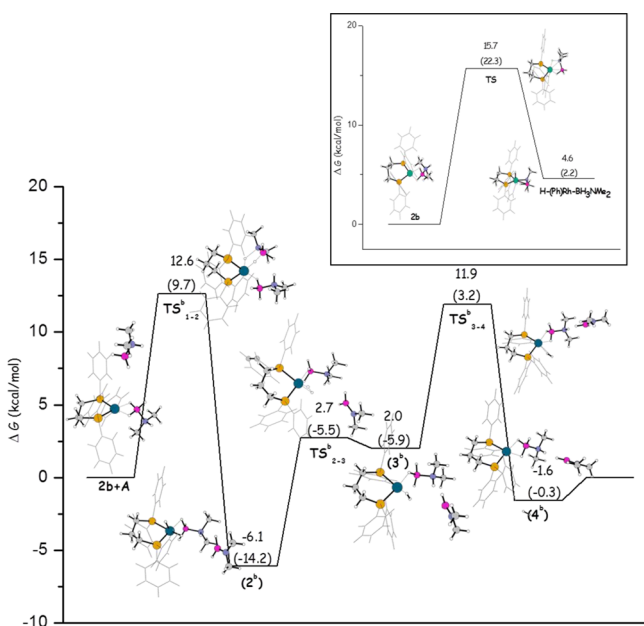
Rh-P=2.242 (2.1992(9))
Rh-B=2.184 (2.199(3))
B-N=1.601
Rh-H=1.820
P1-Rh-P2=94.1 (93)
bite=3.283 (3.32(13))

Figure 6. Calculated B3PW91 free energy profile for the dehydrogenation reaction along the selected dehydrogenation pathway starting from the **2b** complex. Shown on the upper-right side is the pathway for the reaction of the **2b** complex with one substrate molecule. Gas-phase, zero-point-corrected energy changes are reported in parentheses. Energies are in kilocalories per mole and relative to the reactants' asymptote.

used to reduce the preliminary calculation computational efforts, with phenyl rings.

The preliminary results of the computational analysis carried out by using a simplified model of the **2b** catalyst are confirmed. Dehydrogenation of the DMAB molecule coordinated to the Rh center does not occur. As sketched in the framework on the upper-right side of Figure 6, the first NH proton transfer occurs by surmounting an energy barrier of 15.7 kcal/mol and leads to the formation of the H-(Ph)Rh-BH$_3$NH$_2$ intermediate that lies about 4.6 kcal/mol higher in energy than the reference **2b** complex. Further BH hydride transfer and formation of a dihydride complex does not take place, and the only alternative for the formed intermediate to reenter the catalytic cycle is to reform, by overcoming an energy barrier of 11.1 kcal/mol in the reverse direction, the initial complex that can react with a second substrate molecule. Concerted BH hydride and NH proton transfer to the Rh center from the second **A** molecule approaching the **2b** complex occur by overcoming an energy barrier, **TS**$^b_{1-2}$, of 9.7 kcal/mol in the gas phase and 12.6 kcal/mol along the free energy profile. The formed dihydride **2**^{b} complex, from which an aminoborane molecule is released, lies 6.1 kcal/mol (14.2 kcal/mol in gas phase) below the reference energy of separated reactants **2b** + **A**. A free energy barrier of 8.8 kcal/mol for the **TS**$^b_{2-3}$, comparable to the calculated gas-phase barrier of 8.7 kcal/mol, separates the **2**^{b} intermediate from the next minimum **3**^{b} and corresponds to the interaction between the two hydrogen ligands to form a H$_2$ molecule. The formed intermediate **3**^{b} is only slightly more stable than the previous transition state, by 0.7 and 0.4 kcal/mol in solution and gas phase, respectively, and as a consequence, it is less stable than intermediate **2**^{b} by 8.1 kcal/mol in solvent. The elimination of the hydrogen molecule coordinated to the Rh atom from the pseudo-square-planar complex **3**^{b} occurs by overcoming a free energy barrier of 9.9 kcal/mol for the **TS**$^b_{3-4}$.

The corresponding barrier in gas phase is calculated to be 9.1 kcal/mol. The elimination of the H$_2$ molecule along with the coordination mode switch from η^1 to η^2 of the amine-borane ligand leads to the restoration of the initial complex **2b** that is poised to react with a new **A** molecule.

The qualitative behaviors of the **2b(Me)** and **2b** complexes are in agreement, as can be inferred form a comparison of the data reported in Figures 2 and 6. From a quantitative viewpoint, instead, the presence of phosphine ligands bearing the more electron-donating phenyl substituents increases the stability of dihydride and dihydrogen complexes according with previous investigations,[31,35] which have demonstrated how strongly donating bidentate phosphines are able to stabilize complex structures containing hydride and hydrogen ligands. The most important conclusion that we can draw from the outcomes of the present computational investigation is that the active catalyst is the complex formed by displacement in the precatalyst of the

Rh-P=2.251
Rh-B=2.178
B-N=1.588
Rh-H=1.814
P1-Rh-P2=97.6 (96(3))
bite=3.383 3.42(11)

Rh-P=2.256 (2.2141(8))
Rh-B=2.189 (2.189((3))
B-N=1.604
Rh-H=1.837
P1-Rh-P2=99.5 (107(10))
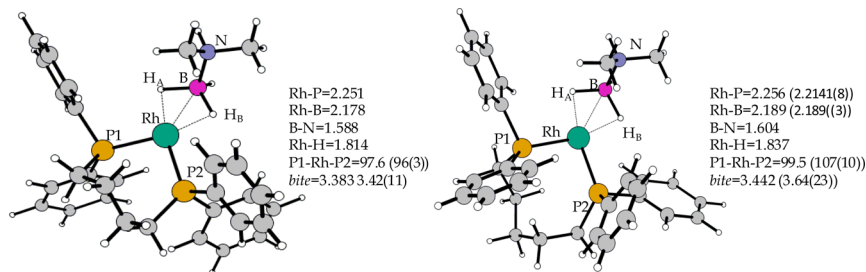*bite*=3.442 (3.64(23))

Figure 7. DFT-optimized geometrical structure of cationic portion of **2c** and **2d**. Selected structural parameters (bonds in angstroms and angles in degrees) are compared with available experimental and estimated values (in parentheses).

fluoroarene ligand and coordination of one substrate molecule. Reaction with a second amine-borane molecule allows the catalytic cycle to start. Release of an aminoborane molecule and molecular hydrogen restore the catalyst that is poised to further react. Off-metal dimerization in solution of released amino-boranes leads to the formation of the cyclic dimer observed product.

Let us describe what happens when the dimethylamine-borane **A** is added to the $[Rh(Ph_2P(CH_2)_n\text{-}PPh_2)(C_6H_5F)]^+$ ($n = 4, 5$) precursors **1c** and **1d** to yield the corresponding **2c** and **2d** complexes and ultimately afford the cyclic amino-borane dimer **C**. The calculated structures of the cationic portion of the **2c** and **2d** complexes are shown in Figure 7. Fully optimized geometrical structures of all the minima and transition states are given in S4 of the SI, along with Cartesian coordinates. The pseudo-square-planar geometry of such complexes is confirmed, with the dimethylamine-borane ligand coordinated to the metal center in an η^2 fashion. As suggested, the increased length of the ligand backbone corresponds to wider P−Rh−P bite angles. The value of 94.1° calculated for the bisphosphine ligand when the number of CH$_2$ units is equal to 3 ($n = 3$) becomes 97.6° and 99.5° for $n = 4$ and 5, respectively. Calculated values reproduce the trend of estimated values of bites and bite angles for such complexes.[29] The Rh−B distances, instead, do not follow the surmised trend. Indeed, the Rh−B bond length decreases in going from $n = 3$ to $n = 4$ and increases again in **2d**, becoming slightly longer than that in **2b**.

The corresponding calculated free energy profiles corrected for the solvent effect are reported in Figure 8 for both **2c** and **2d**
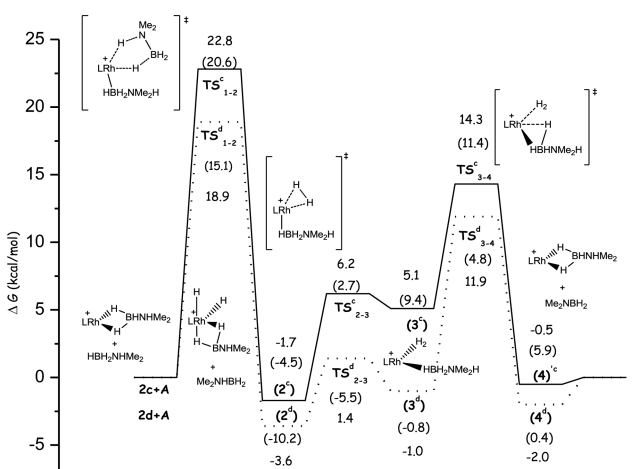

Figure 8. Calculated B3PW91 free energy profiles for the dehydrogen-ation reaction along the selected dehydrogenation pathway starting from the **2c** (solid line) and **2d** (dashed line) complexes. Gas-phase, zero-point-corrected energy changes are reported in parentheses. Energies are in kilocalories per mole and relative to the reactants' asymptote.

complexes. Relative energies in gas phase, reported in parentheses, are not commented. The Supporting Information gives geometrical structures of minima and transition states. The dehydrogenation reaction proceeds by following the same sequence of steps, but by comparison of the energy profiles in Figures 5 and 8, it appears that the relative stabilities of the intercepted stationary points change.

We are going to establish whether these quantitative differences are in agreement with the experimentally observed

catalytic behaviors and support the assumed relationship between structure and reactivity.

After the formation of the **2c** and **2d** σ complexes, the concerted B−H hydride and N−H proton transfer from the second amine-borane molecule **A** to rhodium center occurs through the TS^c_{1-2} and TS^d_{1-2} transition states by overcoming barriers of 22.8 and 18.9 kcal/mol, respectively. The corresponding barrier for the **2b** complex is 12.6 kcal/mol. This first barrier is the highest calculated barrier along the dehydrogenation pathways for all three studied complexes. This means that the concerted NH/BH activation of the second **A** molecule at the metal center represents the rate-determining step of the whole process.

Because all three energy profiles exhibit a very shallow minimum, corresponding to intermediate **3**, according to the suggestion of one of the reviewers of the present work, the stepwise elimination of molecular hydrogen can be considered as a whole, and the total energy barriers calculated considering the difference in energy between **2** minima, a TS_{3-4} transition state. Therefore, the total barriers for the H$_2$ loss are calculated to be 18.2, 16.0, and 15.5 kcal/mol for $n = 1, 2$, and 3, respectively. The first barrier is the highest calculated barrier along the dehydrogenation pathways for **2c** and **2d**, whereas the total barrier for H$_2$ release is the highest for **2b**. This means that the concerted NH/BH activation of the second **A** molecule center represents the rate-determining step (RDS) of the whole process for **2c** ($\Delta E^{\#} = 22.8$ kcal/mol) and **2d** ($\Delta E^{\#} = 18.9$ kcal/mol). Overall dehydrogenation is, instead, the RDS for **2b** ($\Delta E^{\#} = 18.2$ kcal/mol). On the basis of the calculated activation barriers for the RDS by using both approaches, the dehydrogenation rate of **2b**, corresponding to the narrowest bite angle, should be the fastest. The rate decreases in going from **2b** to **2c** and increase again for **2d**. These results are only partially in agreement with experimental findings[27] that, rationalized by invoking the correlation between the bite angle and the strength of the Rh−B interaction, give **2b** as the fastest and **2d** as the slowest.

Aiming at understanding how the amplitude of the bite angle affects the stability of stationary points, we have compared structures and energetics of all three dihydride minima **2** and the TS_{1-2} transition states leading to them. In Figure 9 are sketched
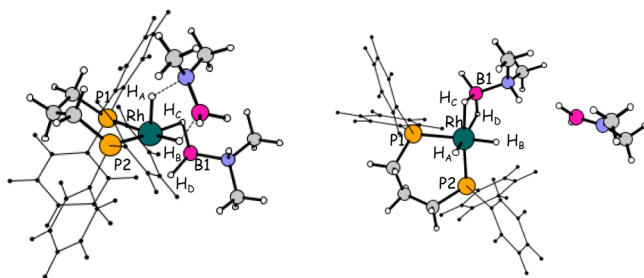

Figure 9. Optimized geometrical structure of the cationic portion of the TS^b and 2^b intermediate. Labels have to be used to read the geometrical information given in Table 1.

the fully optimized structures of the dihydride intermediate 2^b and the transition state TS^b_{1-2} because the reported labels have to be used to read the geometrical information given in Table 1. In this table, the values of some geometrical parameters for both dihydride complexes $[RhH_2(Ph_2P(CH_2)_n\text{-}PPh_2)(\eta_2\text{-}Me_2HNBH_3)]^+$ ($n = 3-5$) and corresponding transition states are given, which can help us to rationalize the computed behaviors. Because of the simultaneous B−H hydride and N−H

Table 1. Calculated Key Geometrical Parameters for 2^b, 2^c, and 2^d Intermediates and Transition States Leading to Them

parameter	TS^b_{1-2}	2^b	TS^c_{1-2}	2^c	TS^d_{1-2}	2^d
P1−Rh−P2 (deg)	92.5	95.7	98.3	98.5	103.8	106.8
H_A-Rh-H_B (deg)	81.1	87.88	80.0	83.3	79.7	83.0
H_A-Rh-P2 (deg)	85.1	171.7	82.5	173.7	80.0	168.2
Rh−B1 (Å)	2.343	2.227	2.335	2.221	2.332	2.218
Rh−P2 (Å)	2.291	2.389	2.305	2.399	2.347	2.450

proton transfer from the second amine-borane molecule **A** to the rhodium center and the switching from a η^2 to η^1 coordination mode of the bound amine-borane molecule, the pseudo-square-planar geometry of the initial complexes **2b**, **2c**, and **2d** becomes square-pyramidal in the transition states. Because one of the transferred H atoms (H_A) occupies an axial position, the angle they form with the Rh center (H_A−Rh−H_B) does not change appreciably with the increase in the diphosphine bite angle (P1−Rh−P2). The larger bite angle instead causes a compression of the angle, in equatorial position, that the second H atom (H_B) forms with the phosphorus labeled P2. At the same time, because the partial detachment of the coordinated amine-borane molecule is required, the strength of the Rh−B bond in **2b**, **2c**, and **2d** complexes has an influence on the height of the barrier for the transition states.

The values of the Rh−B bond length (Rh−B1) are also reported in Table 1 to show the evolution of this geometrical parameter along the reaction coordinate. Because in square-planar **2b**, **2c**, and **2d** the values of the Rh−B distance are 2.184, 2.178, and 2.189 Å, respectively, the observed trend in the barrier heights results from a balance between the geometrical distortion caused by the bite angle enlargement and the influence the bite angle has on the Rh−B interaction strength. The calculated stability ordering of the corresponding minima ($2^b > 2^d > 2^c$) can be rationalized in terms of distortion of the octahedral geometry caused by the widening of the P−Rh−P angle, but compensated by the elongation of the Rh−P bond in the axial position (Rh−P2). The Rh−P bond length in the 2^d intermediate stretched to 2.45 Å indicates that one of the arms of the diphosphine ligand is detached and, consequently, the complex assumes a square pyramidal geometry. The next step of the process is the transformation of dihydride complexes into the corresponding $[Rh(H_2)(Ph_2P(CH_2)_n\text{-}PPh_2)(\eta_2\text{-}Me_2HNBH_3)]^+$ dihydrogen complexes. This transformation proceeds through TS^c_{2-3} and TS^d_{2-3} transition states with barriers of 7.9 and 5.0 kcal/mol, respectively, which are both lower than the analogous barrier of 8.8 kcal/mol calculated along the reaction path for **2b**.

This trend should indicate an enhancing effect of larger bite angles on the rate of a reaction. Relative energies reported in Figures 6 and 8 show that the formed dihydrogen complexes are less stable than the corresponding dihydride complexes. Finally, molecular hydrogen release occurs by overcoming the barriers of 9.2 kcal/mol for TS^c_{3-4} and 12.9 kcal/mol for TS^d_{3-4}. The corresponding energy barrier for the TS^b_{3-4} transition state is 9.9 kcal/mol. Even though the intermediate 4^d, possessing the largest bite angle, appears to be the most reluctant to lose molecular hydrogen, the calculated values of the height of the energy barriers for such and the previous step support the conclusion that, unlike monodentate phosphine systems, Rh(III) chelating-phosphine catalysts rapidly lose hydrogen to reform initial Rh(I) species. The computational exploration carried out in this work supports and reinforces the assumption the use of bidentate chelating phosphine ligands can be beneficial in homogeneous catalysis.

4. CONCLUSIONS

In the framework of a more general project aiming to understand the mechanistic scenario for amine-borane dehydrogenation in more detail, a rigorous quantum-mechanical investigation of the dehydrocoupling reaction of the secondary amine-borane Me_2HNBH_3 assisted by phosphine chelating $[Rh(Ph_2P(CH_2)_n\text{-}PPh_2)(C_6H_5F)]^+$ ($n = 3-5$) complexes to ultimately afford the cyclic dimer $[Me_2NBH_2]_2$ has been reported. An accurate exploration of all the viable dehydrocoupling pathways has been carried out. The dehydrogenation pathway that, on the basis of the computed results, appears to be the most viable involves, as the first step, the concerted B−H hydride and N−H proton transfer from an additional amine-borane molecule to the rhodium center of the formed $[Rh(Ph_2P(CH_2)_n\text{-}PPh_2)(\eta_2\text{-}Me_2HNBH_3)]^+$ complexes. The reaction proceeds by formation of dihydrogen complexes, which eliminate molecular hydrogen and restore the σ-amine-borane complexes, which are poised to react with a new dimethylamine-borane molecule. Off-metal coupling of the released aminoborane molecules leads to the formation of the final cyclic product. The step that gives the formation of dihydride complexes has been calculated to be the rate-determining step of the whole process for **2c** and **2d** complexes, whereas overall H_2 loss is the slowest step along the dehydrogenation pathway for **2b**.

How the amplitude of the P−Rh−P bite angle influences the stability of intercepted stationary points has been investigated. The impact that the length of the diphosphine ligand backbone has on every step of the process has been equally examined. According to conclusions coming from experimental evidence, the elimination of molecular hydrogen from the studied complexes is calculated to involve energy barriers low enough to allow the restoration of initial Rh(I) catalysts.

Concerning the observation of an induction period, which has been hypothesized to be due to the formation of a dimeric species in equilibrium with monomers, our calculations do not support this hypothesis.

The trends observed for the systems studied above provide additional information to the more general context of metal-assisted amine-borane dehydrocoupling processes. Future studies will address the influence that the identity of the metal has on both the rate of catalysis and the intermediates to supply yet more information on this important transformation.

■ ASSOCIATED CONTENT

Ⓢ Supporting Information

Atomic coordinates and absolute energies of all optimized stationary points and transition states. This material is available free of charge via the Internet at http://pubs.acs.org.

■ AUTHOR INFORMATION

Corresponding Author

*E-mail: siciliae@unical.it.

Notes

The authors declare no competing financial interest.

REFERENCES

(1) Leitao, E. M.; Jurca, T.; Manners, I. *Nat. Chem.* **2013**, *5*, 817−829.

(2) Staubitz, A.; Robertson, A. P. M.; Manners, I. *Chem. Rev.* **2010**, *110*, 4079−4124.

(3) Hamilton, C. W.; Baker, R. T.; Staubitz, A.; Manners, I. *Chem. Soc. Rev.* **2009**, *38*, 279−293.

(4) Staubitz, A.; Soto, A. P.; Manners, I. *Angew. Chem.* **2008**, *47*, 6212−6215.

(5) Keaton, R. J.; Blacquiere, J. M.; Baker, R. T. *J. Am. Chem. Soc.* **2007**, *129*, 1844.

(6) Hill, M. S.; Hodgson, M.; Liptrot, D. J.; Mahon, M. F. *Dalton Trans.* **2011**, *40*, 7783.

(7) Kawano, Y.; Uruichi, M.; Shimoi, M.; Taki, S.; Kawaguchi, T.; Kakizawa, T.; Ogino, H. *J. Am. Chem. Soc.* **2009**, *131*, 14946.

(8) Chapman, A. M.; Haddow, M. F.; Wass, D. F. *J. Am. Chem. Soc.* **2011**, *133*, 8826.

(9) Hill, M. S.; Kociok-Koehn, G.; Robinson, T. P. *Chem. Commun.* **2010**, *46*, 7587.

(10) Miyazaki, T.; Tanabe, Y.; Yuki, M.; Miyake, Y.; Nishibayashi, Y. *Organometallics* **2011**, *30*, 2394.

(11) Sloan, M. E.; Staubitz, A.; Clark, T. J.; Russell, C. A.; Lloyd Jones, G. C.; Manners, I. *J. Am. Chem. Soc.* **2010**, *132*, 3831.

(12) Pun, D.; Lobkovsky, E.; Chirik, P. J. *Chem. Commun.* **2007**, 3297.

(13) MacInnis, M. C.; McDonald, R.; Ferguson, M. J.; Tobisch, S.; Turculet, L. *J. Am. Chem. Soc.* **2011**, *133*, 13622.

(14) Vance, J. R.; Robertson, A. P. M; Lee, K.; Manners, I. *Chem.—Eur. J.* **2011**, *17*, 4099.

(15) Ledger, A. E. W.; Ellul, C. E.; Mahon, M. F.; Williams, J. M. J.; Whittlesey, M. K. *Chem.—Eur. J.* **2011**, *17*, 8704.

(16) Alcaraz, G.; Grellier, M.; Sabo-Etienne, S. *Acc. Chem. Res.* **2009**, *42*, 1640.

(17) Jiang, Y.; Hess, J.; Fox, T.; Berke, H. *J. Am. Chem. Soc.* **2010**, *132*, 18233.

(18) Zimmerman, P. M.; Paul, A.; Zhang, Z. Y.; Musgrave, C. B. *Inorg. Chem.* **2009**, *48*, 1069.

(19) Butera, V.; Russo, N.; Sicilia, E. *Chem.—Eur. J.* **2011**, *17*, 14586.

(20) Sloan, M. E.; Clark, T. J.; Manners, I. *Inorg. Chem.* **2009**, *48*, 2429.

(21) Jaska, C. A.; Temple, K.; Lough, A. J.; Manners, I. *J. Am. Chem. Soc.* **2003**, *125*, 9424.

(22) Vogt, M.; de Bruin, B.; Berke, H.; Trincado, M.; Grutzmacher, H. *Chem. Sci.* **2011**, *2*, 723.

(23) Tang, C. Y.; Thompson, A. L.; Aldridge, S. *J. Am. Chem. Soc.* **2010**, *132*, 10578.

(24) Rousseau, R.; Schenter, G. K.; Fulton, J. L.; Linehan, J. C.; Engelhard, M. H.; Autrey, T. *J. Am. Chem. Soc.* **2009**, *131*, 10516.

(25) Fulton, J. L.; Linehan, J. C.; Autrey, T.; Balasubramanian, M.; Chen, Y.; Szymczak, N. K. *J. Am. Chem. Soc.* **2007**, *129*, 11936.

(26) Sewell, L. J.; Lloyd-Jones, G. C.; Weller, A. S. *J. Am. Chem. Soc.* **2012**, *134*, 3598.

(27) Dallanegra, R.; Robertson, A. P. M; Chaplin, A. B.; Manners, I.; Weller, A. S. *Chem. Commun.* **2011**, *47*, 3763.

(28) Casey, C. P.; Whiteker, G. T. *Isr. J. Chem.* **1990**, *30*, 299.

(29) Aguilà, D.; Escribano, E.; Speed, S.; Talancón, D.; Yermán, L.; Alvarez, S. *Dalton Trans.* **2009**, 6610.

(30) Halpern, J.; Riley, D. P.; Chan, A. S. C.; Pluth, J. J. *J. Am. Chem. Soc.* **1977**, *99*, 8055.

(31) Marcone, J. E.; Moloy, K. G. *J. Am. Chem. Soc.* **1998**, *120*, 8527.

(32) Wilson, A. D.; Miller, A. J. M.; DuBois, D. L.; Labinger, J. A.; Bercaw, J. E. *Inorg. Chem.* **2010**, *49*, 3918.

(33) Birkholz, M. N.; Freixa, Z.; van Leeuwen, P. W. N. M. *Chem. Soc. Rev.* **2009**, *38*, 1099.

(34) van Zeist, W. J.; Visser, R.; Bickelhaupt, F. *Chem.—Eur. J.* **2009**, *15*, 6112.

(35) Freixa, Z.; van Leeuwen, P. W. N. M. *Dalton Trans.* **2003**, 1890.

(36) Lovitt, C. F.; Frenking, G.; Girolami, G. S. *Organometallics* **2012**, *31*, 4122.

(37) Frisch, M. J.; Trucks, G. W.; Schlegel, H. B.; Scuseria, G. E.; Robb, M. A.; Cheeseman, J. R.; Montgomery, J. A., Jr.; Vreven, T.; Kudin, K. N.; Burant, J. C.; Millam, J. M.; Iyengar, S. S.; Tomasi, J.; Barone, V.; Mennucci, B.; Cossi, M.; Scalmani, G.; Rega, N.; Petersson, G. A.; Nakatsuji, H.; Hada, M.; Ehara, M.; Toyota, K.; Fukuda, R.; Hasegawa, J.; Ishida, M.; Nakajima, T.; Honda, Y.; Kitao, O.; Nakai, H.; Klene, M.; Li, X.; Knox, J. E.; Hratchian, H. P.; Cross, J. B.; Bakken, V.; Adamo, C.; Jaramillo, J.; Gomperts, R.; Stratmann, R. E.; Yazyev, O.; Austin, A. J.; Cammi, R.; Pomelli, C.; Ochterski, J. W.; Ayala, P. Y.; Morokuma, K.; Voth, G. A.; Salvador, P.; Dannenberg, J.J.; Zakrzewski, V. G.; Dapprich, S.; Daniels, A. D.; Strain, M. C.; Farkas, O.; Malick, D. K.; Rabuck, A. D.; Raghavachari, K.; Foresman, J. B.; Ortiz, J. V.; Cui, Q.; Baboul, A. G.; Clifford, S.; Cioslowski, J.; Stefanov, B. B.; Liu, G.; Liashenko, A.; Piskorz, P.; Komaromi, I.; Martin, R. L.; Fox, D. J.; Keith, T.; Al-Laham, M. A.; Peng, C. Y.; Nanayakkara, A.; Challacombe, M.; Gill, P. M. W.; Johnson, B.; Chen, W.; Wong, M. W.; Gonzalez, C.; Pople, J. A. *Gaussian 03, revision B.05*; Gaussian, Inc.: Wallingford, CT, 2004.

(38) (a) Becke, A. D. *J. Chem. Phys.* **1993**, *98*, 5648. (b) Perdew, J. P.; Wang, Y. *Phys. Rev. B* **1992**, *45*, 13244.

(39) Andrae, D.; Häußermann, U.; Dolg, M.; Stoll, H.; Preuß, H. *Teor. Chim. Acta* **1990**, *77*, 123.

(40) Becke, A. D. *J. Chem. Phys.* **1997**, *107*, 8554.

(41) Chai, J.-D.; Head-Gordon, M. *Phys. Chem. Chem. Phys.* **2008**, *10*, 6615.

(42) (a) Fukui, K. *J. Phys. Chem.* **1970**, *74*, 4161. (b) Gonzalez, C.; Schlegel, H. B. *J. Chem. Phys.* **1989**, *90*, 2154.

(43) Cooper, J.; Ziegler, T. *Inorg. Chem.* **2002**, *41*, 6614.

(44) Tobisch, S. *Chem.-Eur. J* **2005**, *11*, 3113.

(45) (a) Cancès, M. T.; Mennucci, B.; Tomasi, J. *J. Chem. Phys.* **1997**, *107*, 3032. (b) Cossi, M.; Barone, V.; Mennucci, B.; Tomasi, J. *Chem. Phys. Lett.* **1998**, *286*, 253. (c) Mennucci, B.; Tomasi, J. *J. Chem. Phys.* **1997**, *106*, 5151.

(46) Kollaman, P. *Chem Rev* **1993**, *93*, 2395.

(47) Chaplin, A. B.; Weller, A. S. *Angew. Chem., Int. Ed.* **2010**, *49*, 581.

(48) (a) Liu, J.; Wang, H.; Zhang, H.; Wu, X.; Deng, Y.; Yang, Z.; Lei, A. *Chem.−Eur. J.* **2009**, *15*, 4437. (b) Conley, B. L.; Williams, T. J. *Chem. Commun.* **2010**, *46*, 4815.